2026 IEEE International Conference on Robotics and Automation (ICRA 2026)
June 1-5, 2026. Vienna, Austria

Decoding Multi-Finger Motions and Grasp Types with Grasp-Specific Models and Lightmyography Based Muscle-Machine Interfaces

Zhe Wang, Bonnie Guan, Shifei Duan, Kean C. Aw, and Minas Liarokapis

***Abstract*— Efficiently decoding human movement and/or intention is essential for controlling advanced prosthetic and robotic systems. Various muscle-machine interfaces have been researched for this purpose, including electromyography and lightmyography based interfaces. However, the decoding effectiveness of lightmyography signals for multi-finger hand motions remains insufficiently explored. This study investigates the decoding of human multi-finger movements using different machine learning methods. Lightmyography and finger motion data were collected from six participants grasping five common objects. Data were preprocessed using the sliding window method and decoded using three machine learning algorithms: random forest, convolutional neural networks, and multi-layer perceptron. Moreover, models were trained in a grasp-specific manner increasing decoding accuracy. Finally, statistical analysis demonstrated that the random forest model significantly outperformed the other methods, establishing it as the most suitable technique for decoding multi-finger motions from lightmyography signals.**

I. INTRODUCTION

Muscle-Machine Interfaces (MuMIs) are a class of human-machine interfaces that have been widely applied in various interactive applications, such as smart prosthetics, exoskeletons, and rehabilitation devices. MuMIs function by capturing muscle activity through various sensing modalities to decode human motor intent, ultimately controlling actuators to facilitate human-machine interaction. The most common approach to developing MuMIs involves using surface Electromyography (sEMG) to decode human gestures, which are then translated into control commands for prosthetic or robotic hands [1]. However, sEMG signals are susceptible to several disadvantages, including interference from electromagnetic noise, sensitivity to electrode placement, and signal noise from sweat or hair.

Consequently, numerous novel MuMIs have been proposed to provide affordable and robust alternatives to sEMG. Forcemyography (FMG), which measures the surface pressure profile exerted by contracting muscles, has been proposed as one such alternative [2], [3]. Another interface that detects the mechanical properties of muscle activity is mechanomyography (MMG), which records and quantifies the low-frequency lateral oscillations of active skeletal muscle fibers [4]. Compared to sEMG, which can capture the deep electrical activity of muscles, both FMG and MMG are primarily limited to detecting information from the superficial layers of the skin. Sonomyography (SMG), which leverages ultrasound to detect morphological changes in underlying soft tissues, can obtain information from individual muscles and tendons at various depths [5]. However, this method requires bulky and expensive equipment. Recently, a novel MuMI called Lightmyography (LMG) was proposed [6]. LMG emits light at different wavelengths and utilizes photosensors to measure light reflection from the skin and underlying muscle, allowing for the measurement of muscle displacement. As demonstrated in [6], LMG achieves competitive classification performance relative to EMG for five-gesture decoding tasks. Furthermore, LMG can be implemented at low cost and shows increased robustness to electromagnetic interference [7]. Further details on the principles of LMG and the influence of different wavelengths can be found in [8], [9].

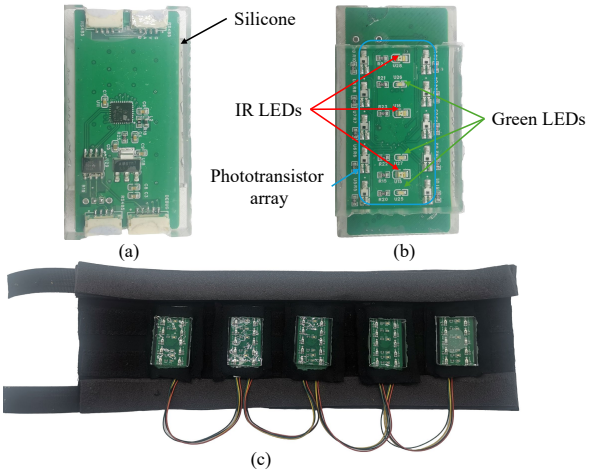

Fig. 1. LMG module and armband. Each module is equipped with three green LEDs, three infrared LEDs, and an array of 5x2 phototransistors. Subfig. a) presents the back side of LMG Module. Subfig. b) presents the front side of LMG Module. Subfig. c) presents the LMG armband with five modules.

Hand gesture classification and continuous hand motion prediction are standard tasks for assessing the decoding of human movement intentions. Numerous studies have demonstrated high accuracy gesture recognition (over 85%) using various MuMIs [10]–[13]. Abbas et al. [10] extracted 12 descriptive statistical features from MMG signals and evaluated them using five different machine learning (ML) methods. Their results show that the support vector machine

Zhe Wang, Bonnie Guan and Shifei Duan are with the New Dexterity research group, Department of Mechanical and Mechatronics Engineering, The University of Auckland, New Zealand. {zwan341, bgua324, sdua078}@aucklanduni.ac.nz

Kean C. Aw is with the Department of Mechanical and Mechatronics Engineering, The University of Auckland, New Zealand. k.aw@auckland.ac.nz

Minas Liarokapis is with the New Dexterity research group, The University of Auckland, New Zealand and the National Technical University of Athens, Greece. liarokapis@mail.ntua.gr

outperformed the other methods, achieving an accuracy of 97.1%. Vásconez et al. [11] compared reinforcement learning and supervised ML for hand gesture recognition on their public sEMG dataset. Their results show that supervised learning methods outperform reinforcement learning methods for user-general gesture classification systems. Godoy et al. [13] achieved an accuracy of 92% in classifying 32 distinct hand gestures from LMG data using a novel deep learning technique called the Temporal Multi-Channel Vision Transformer. In addition to gesture classification, the continuous prediction of hand motion offers a more intuitive and synchronous method for controlling prosthetic or robotic hands by directly mapping joint angles. Numerous studies have explored continuous joint angle prediction using different MuMIs [14]–[16]. Zhang et al. [14] proposed a continuous Kalman estimation method for sEMG-based finger kinematics prediction, achieving an average computation time below 0.01 seconds. This represents a substantial improvement over deep learning and neural network approaches and highlights its potential for real-time finger motion mapping. Bimbraw et al. [15] investigated hand motion recognition using forearm ultrasound, achieving accurate and low-latency estimation of hand configurations and joint angles, thereby suggesting the feasibility of real-time control based on ultrasound. Chen et al. [16] used a hybrid sEMG-FMG modality to predict joint angles of five fingers during six different hand movements. These works collectively demonstrate the effectiveness of various MuMIs for predicting finger motion. However, to the best of our knowledge, the continuous prediction of hand motions using LMG has not yet been investigated, leaving its efficacy for this task unknown.

In this work, we address this gap by collecting a dataset from six participants performing grasping motions with five common household objects. This dataset includes both the flexion/extension angles of all five fingers and synchronously recorded LMG data. As ML is the most prevalent method for decoding MuMI data, this study evaluates the performance of different ML techniques to identify the most suitable approach for LMG-based finger motion prediction. Additionally, we assess the classification performance of the corresponding grasp types.

The rest of this paper is organized as follows. Section II presents the experimental setup, the novel LMG sensor design, the data collection protocol, and the selected Machine Learning techniques, including their training and evaluation methods. Section III provides the results for grasp type classification and continuous motion prediction, followed by an analysis of these results, a discussion of the study's limitations, and directions for future work. Finally, Section IV concludes the paper.

II. METHODS

A. Experimental Setup

To acquire multi-channel LMG data for decoding hand grasp types and finger motions, a new LMG module was proposed. Compared with the design in [7], the new module features a rigid structure encapsulated in silicone. Each module

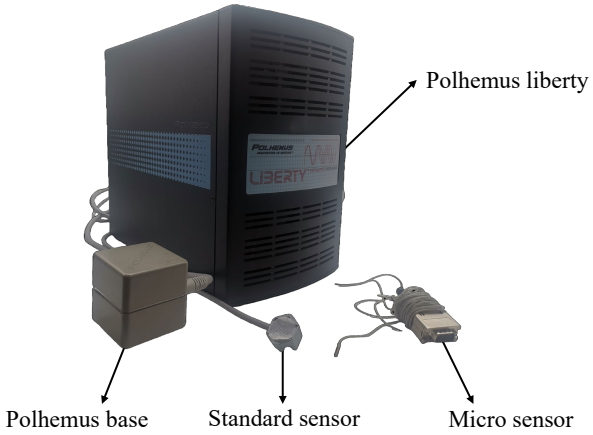

Fig. 2. Polhemus Liberty magnetic motion capture system.

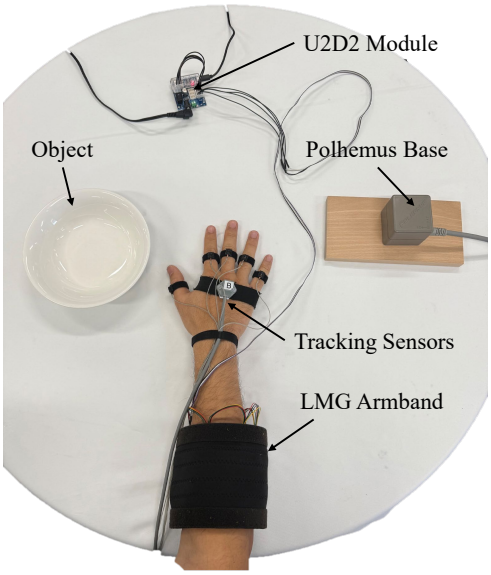

Fig. 3. Experimental setup used in this study. The LMG armband is attached on the forearm, and the magnetic motion tracking sensors are attached to the human palm and fingers.

is controlled by an STM32L432 microcontroller that drives the green and infrared LEDs and acquires analog-to-digital (AD) data from 10 phototransistors, enabling ten-channel signal acquisition per module. Modules communicate via an RS485 bus, transmitting the combined data to a host computer through a U2D2 interface from DYNAMIXEL. A five-module configuration achieves a stable sampling frequency of 50 Hz. The LMG armband incorporates a fabric sleeve to hold the modules. To enhance versatility, a daisy-chain design was also implemented, enabling the modules to be used not only as a circumferential armband but also individually for targeted measurements of specific muscles. The complete LMG module and armband are shown in Fig. 1.

The ground truth finger motion data were captured using a Polhemus Liberty magnetic motion capture system, shown in Fig. 2. This system comprised five micro sensors and one standard sensor. The standard sensor was placed on the sub-

(a) Screwdriver (b) Cup (c) Bowl (d) Ball (e) Bottle

Fig. 4. Objects used in the experiment and their corresponding grasp gestures.

TABLE I

SUBJECT INFORMATION. *SUBJ.* STANDS FOR SUBJECT, *M* STANDS FOR MALE, *F* FOR FEMALE, AND *HAND.* FOR HANDEDNESS.

Subj.	1	2	3	4	5	6
Age	27	29	27	27	32	26
Sex	M	M	F	M	M	M
Hand	Right	Right	Right	Right	Right	Right

ject's dorsum (back of the hand) to serve as a reference, while the five micro sensors were placed on each finger between the Proximal Interphalangeal (PIP) and Metacarpophalangeal (MCP) joints. These are tracking sensors as shown in Fig. 3. The system was configured to sample at 50 Hz to match the sampling rate of the LMG data. The coordinate frame of the hand-mounted sensor served as the reference frame. The flexion/extension (flex/ext) angle of each finger was then computed by calculating the rotation of its respective micro-sensor's frame relative to this reference frame. The complete experimental setup is presented in Fig. 3, where the LMG armband and tracking sensors are placed on the subject's forearm and hand, respectively.

B. Data Collection

The study was approved by the institutional Human Participants Ethics Committee (Reference #26227), and all experiments were conducted in accordance with relevant guidelines and regulations. All six participants provided written informed consent prior to the experiment. Detailed information for each participant is provided in Table I. During the experiment, the LMG armband was positioned on the forearm of each participants and the motion capture sensors on their hand. The experimental protocol for each object consisted of a repeating trial structure: a 5-second rest period followed by a 7-second movement period. During the movement period, participants were instructed to reach for an object, grasp it naturally, lift it, place it back down, and return their hand to the starting position. This entire sequence constituted one trial. Each trial was repeated 10 times per object. Visual cues displayed on a computer screen indicated the transitions between rest and movement phases. Participants were permitted to rest if they experienced fatigue during the data collection session. Five objects were selected for the study because they are frequently used in daily activities and require distinct five-finger grasp patterns. The specific grasp types for the selected objects were as follows: Screwdriver (Palmar Pinch), Cup (Lateral), Bowl (Extension-type), Ball (Power Sphere), and Bottle (Medium Wrap). These grasp types were chosen from the taxonomy in [17] and represent grasps commonly used for these objects in the execution of daily activities. The objects and the corresponding grasps are shown in Fig. 4.

C. Data Preprocessing

The LMG data were pre-processed before being used to train the machine learning models. Unlike traditional EMG processing approaches, LMG pre-processing steps did not include signal filtering or hand-crafted feature extraction. Normalization was also omitted from the pre-processing pipeline, as batch normalization layers were integrated directly into the neural network. This technique normalizes the input for each training mini-batch, which can improve training speed and performance [18]. To generate samples for the models, we used a sliding window of 200 ms with a 20 ms stride across the LMG time-series data. The window size was selected to be larger than the 125 ms minimum suggested by [19] to reduce bias and variance, yet smaller than the 300 ms maximum recommended for real-time prosthetic control [20]. The resulting dataset was balanced to prevent model bias towards any single class. This was achieved by randomly downsampling the majority classes until all classes contained an equal number of samples. For the finger motion data, which served as the ground truth for regression models, we applied a moving average filter using the current and four preceding time steps. After windowing, a target label was assigned to each window for the classification and regression tasks. For the classification tasks, the label of the central time point within each window was assigned to the entire window. For the regression tasks, the target value was the average of the angles across all time steps within the window.

D. ML Methods for Classification & Regression

Three ML methods were employed to both classify grasp types and predict finger motion data. The classical method chosen was Random Forest (RF) [21]. RF is selected for its computational efficiency, its inherent ability to handle both multi-class classification and multi-output regression problems, and its general robustness. RF is an ensemble learning method that constructs a multitude of decision trees during training. For classification tasks, the final output is determined by the majority vote among the individual trees. For regression, the output is the mean of the predictions from

all trees. The number of trees was set to 100, and other hyperparameters were left at their default values.

The first neural network evaluated was a Multi-Layer Perceptron (MLP), a type of Artificial Neural Network (ANN). A key advantage of this architecture is their ability to model complex, non-linear relationships between input signals and output tasks [19]. The specific MLP employed in this study consisted of an input layer followed by three fully-connected (dense) hidden layers. To improve training stability and prevent overfitting, each hidden layer was followed by a batch normalization layer and a dropout layer. The final dense layer generated the output: for grasp classification, it used a softmax activation function; for motion data regression, it used a linear activation function. The second neural network evaluated was a Convolutional Neural Network (CNN) [22], which is widely used for biomedical signal processing due to its effectiveness in automatically extracting features. The model architecture began with three one-dimensional convolutional layers, each followed by a batch normalization and a dropout layer. These layers processed the raw LMG signals to learn hierarchical temporal features. The output feature maps from the convolutional blocks were then flattened and passed to a series of dense layers, which also included dropout for regularization. Similar to the MLP, a final dense output layer used a softmax activation for classification or a linear activation for regression.

E. Training and Evaluation

For each subject, we addressed two distinct decoding tasks: grasp classification and continuous finger motion regression. For the grasp classification task, a single classifier was trained for each machine learning architectures (i.e., CNN, RF, MLP). These models were trained on a dataset containing data from all five objects. This approach was taken to evaluate the models' ability to generalize across different grasp types. For the finger motion regression task, two different modeling strategies were employed:

- Grasp-Specific Regressors: Separate regressors were trained for each grasp type to capture subtle finger-motion variations caused by differences in object size and shape, even when the grasp type is the same.
- Generalized Regressor: A single regressor was trained on the combined data from all objects. This model was used to evaluate the general regression capabilities of the three machine learning architectures.

All mentioned models were implemented using Python with the Scikit-learn library for RF and TensorFlow/Keras for CNN and MLP. The models were trained and evaluated using a 10-fold cross-validation scheme based on the experimental repetitions. Specifically, for each fold, one of the ten repetitions was held out as the test set, while the remaining nine were used for training. This process was repeated ten times, ensuring that each repetition was used as the test set exactly once. For the neural network models (CNN and MLP), the training was configured as follows:

- Loss Function: Categorical Cross-Entropy for classification tasks and Mean Squared Error for regression tasks.

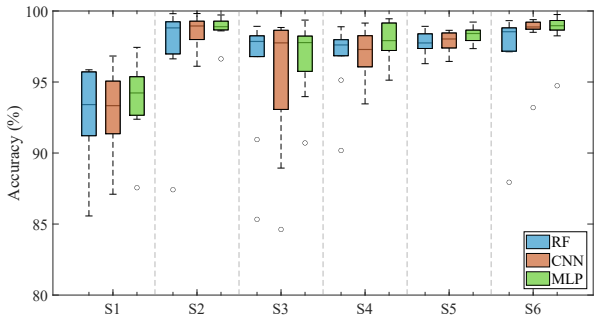

Fig. 5. Boxplots comparing the classification accuracy of the different decoding models for each subject. The distribution shown in each boxplot is generated from the accuracies of the ten-fold cross-validation process.

TABLE II

OVERALL DECODING ACCURACIES IN PERCENTAGE. *AVG* STANDS FOR AVERAGE AND *STD* STANDS FOR SAMPLE STANDARD DEVIATION.THE GREATER ACCURACY FOR EACH SUBJECT IS HIGHLIGHTED IN GREEN.

RF						
Subj.	**1**	**2**	**3**	**4**	**5**	**6**
AVG	92.79	97.45	95.98	96.80	97.80	97.29
STD	3.27	3.67	4.38	2.54	0.79	3.36
CNN						
AVG	92.94	98.56	95.40	97.01	97.89	98.39
STD	3.04	1.17	4.95	1.71	0.68	1.84
MLP						
AVG	93.95	98.81	96.73	97.76	98.33	98.62
STD	2.76	0.87	2.64	1.48	0.52	1.43

- Optimizer: The Adam optimizer [23] was employed to update the model weights during training for all neural network models.

Classification performance was evaluated using accuracy. Regression performance was assessed using three standard metrics: the coefficient of determination (R^2), the correlation coefficient (CC), and the root mean squared error ($RMSE$).

III. RESULTS AND DISCUSSION

A. Prediction of Hand Grasp Types

The grasp classification performance is broken down by subject in Fig. 5, which displays the accuracy for each participant. For a detailed comparison of the models' overall performance, refer to Table II.

As shown in Fig. 5, there is clear inter-subject variability in classification performance. For instance, subjects S5 and S6 achieved consistently higher accuracies, whereas the performance for subject S1 was comparatively lower. This variability is expected, as musculoskeletal characteristics vary significantly across subjects. The boxplots for subjects S3 and S6 also show outliers for all three models. This is likely due to intra-subject variability in how a motion is executed across repetitions. Rather than being an experimental artifact, this variability reflects realistic human movement and poses an inherent challenge that decoding models must address. In terms of performance stability, the smaller interquartile ranges for the MLP model on subjects S1, S2, and S5 suggest it provided more consistent predictions for these individuals.

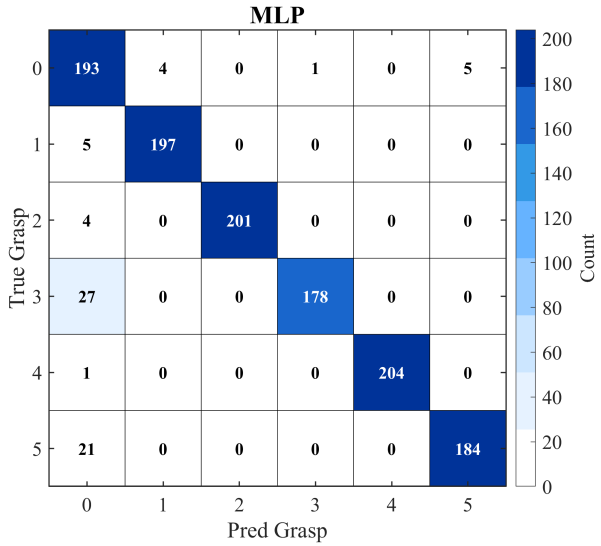

Fig. 6. Confusion matrix showing the decoding accuracy for each of the five grasp types and rest posture achieved by the MLP model.

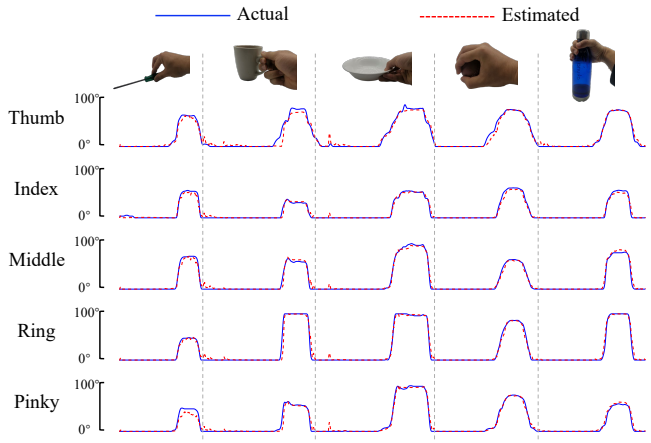

Fig. 7. A representative example of finger motion predictions made by the RF model for a single subject. The plot shows the predicted (red) and actual (blue) flexion angles of the five fingers over time during a test fold.

Considering the average accuracies summarized in Table II, the MLP model demonstrates superior decoding accuracy and lower standard deviation compared to both the RF and CNN models. It achieved a mean accuracy of 98.81% for classifying the five grasp types. Notably, all three models achieved high mean accuracies of exceeding 92% across all subjects. A representative confusion matrix for the MLP model's performance on a single subject is shown in Fig. 6.

To statistically compare the performance of the three models, a one-way repeated measures ANOVA was conducted [24]. The results revealed a significant main effect of model type on classification accuracy ($F(2, 10) = 13.35$, $p = 0.0015$), indicating that the choice of classifier had a significant impact on decoding performance. Post-hoc pairwise comparisons with Bonferroni correction were performed to further investigate the differences [25]. These analyses indicated that the MLP model significantly outperformed both the CNN ($p = 0.01$) and RF ($p = 0.0007$) models. In contrast, there was no significant difference between the CNN and RF models ($p = 0.24$). These results suggest that the MLP model is more effective for decoding hand grasp types from LMG signals compared to the other two models. Given this performance, a real-time implementation strategy could involve using the MLP as a trigger to select grasp-specific regressors.

B. Estimation of Hand Motions

Overall, Fig. 7 illustrates a representative example of the finger motion predictions produced by the RF model for a single subject. As shown in the figure, the RF model accurately estimates the motion of the five fingers across five distinct grasp types. To further compare the two modeling strategies, the results are presented as follows.

The performance of the five grasp-specific regressors for each subject is summarized in Fig. 8 and Table III. These results indicate that all models achieved consistently reliable performance across different subjects, demonstrating high average accuracy ($R^2 \geq 0.89$), strong correlation with the ground truth ($CC > 0.97$), and low prediction error ($RMSE < 6.5°$). This level of performance shows that the models can explain a large portion of the variance in finger flexion angles, accurately capture the dynamics of hand movement, and maintain a low prediction error. To further investigate the effect of model selection on regression performance, a one-way repeated measures ANOVA was performed. The analysis revealed a significant main effect of model type across all three evaluation metrics: R^2 ($p = 0.006$), CC ($p = 0.038$), and $RMSE$ ($p = 0.011$). Post-hoc pairwise comparisons with Bonferroni correction were performed to further investigate these differences. These analyses consistently showed that the RF model performed significantly better than the CNN and MLP models. Specifically, RF significantly outperformed CNN ($p = 0.037$) and MLP ($p = 0.023$) for the R^2 metric, and over CNN ($p = 0.030$) and MLP ($p = 0.045$) for the $RMSE$ metric. For the CC metric, RF significantly outperformed CNN ($p = 0.016$). In contrast, the performance difference between CNN and MLP was not statistically significant for any metric ($p > 0.37$).

The performance of a generalized regressor trained on data from all objects considered in this study was also evaluated, as shown in Fig. 9 and Table IV. As shown in Fig. 9, the performance distribution for the RF model exhibits a larger interquartile range for some subjects. This variance likely reflects the subtle natural differences in the flexion angles of the fingers that occur in repeated tests. In general, the generalized regressors trained with the three machine learning techniques performed exceptionally well for all subjects, achieving R^2 values above 0.9 and $RMSE$ values below 6.5°. The same statistical analysis as above was performed to compare the performance of the three techniques. The analysis revealed a highly significant main effect of model type across all metrics: R^2 ($F(2, 10) = 20.72$, $p < 0.001$), CC ($F(2, 10) = 24.94$, $p < 0.001$), and RMSE ($F(2, 10) = 26.94$, $p < 0.001$). Post-hoc paired comparisons confirmed a clear and consistent performance hierarchy. For all three metrics, the RF model

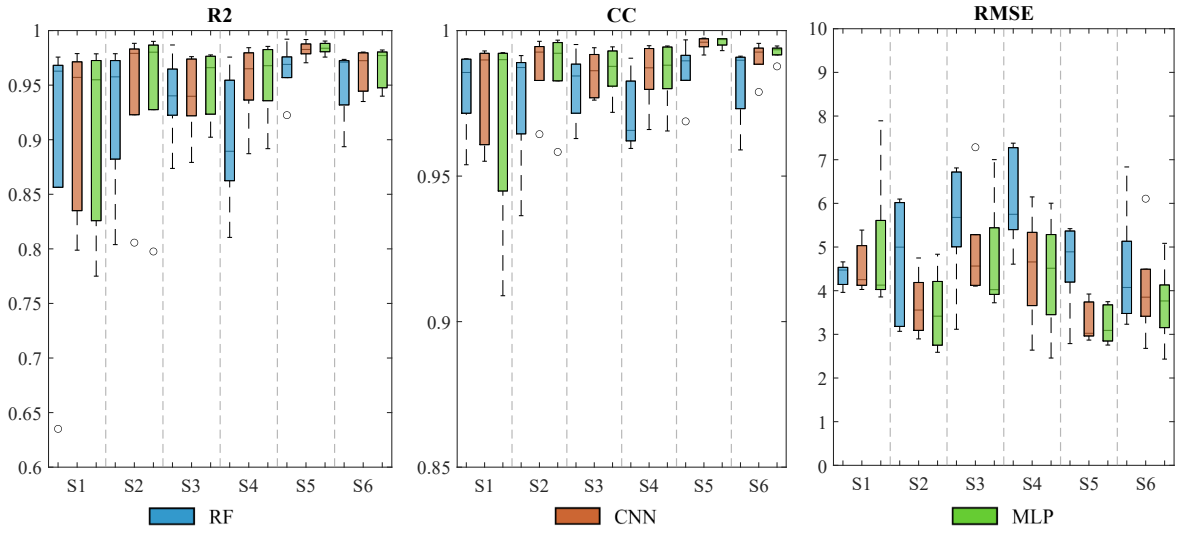

Fig. 8. Boxplots comparing the regression performance of the different decoding models for each subject, evaluated under three distinct metrics. Each boxplot shows the performance distribution generated from the scores of the five grasp-specific regression models.

TABLE III

OVERALL GRASP-SPECIFIC MODEL DECODING PERFORMANCE IN THREE METRICS. *AVG* STANDS FOR AVERAGE AND *STD* STANDS FOR SAMPLE STANDARD DEVIATION.

	R2						**CC**						**RMSE**					
	RF						**RF**						**RF**					
Subj.	**1**	**2**	**3**	**4**	**5**	**6**	**1**	**2**	**3**	**4**	**5**	**6**	**1**	**2**	**3**	**4**	**5**	**6**
AVG	0.89	0.92	0.94	0.90	0.96	0.95	0.98	0.98	0.98	0.97	0.99	0.98	4.36	4.68	5.59	6.13	4.62	4.45
STD	0.15	0.07	0.04	0.06	0.03	0.03	0.02	0.02	0.01	0.01	0.01	0.01	0.28	1.46	1.48	1.17	1.07	1.42
	CNN						**CNN**						**CNN**					
AVG	0.91	0.94	0.94	0.95	0.98	0.96	0.98	0.99	0.98	0.99	1.00	0.99	4.55	3.67	4.94	4.50	3.30	4.05
STD	0.08	0.08	0.04	0.04	0.01	0.02	0.02	0.01	0.01	0.01	0.01	0.01	0.58	0.73	1.33	1.30	0.47	1.26
	MLP						**MLP**						**MLP**					
AVG	0.90	0.94	0.95	0.96	0.98	0.97	0.97	0.99	0.99	0.99	1.00	0.99	4.96	3.53	4.73	4.36	3.22	3.70
STD	0.09	0.08	0.03	0.03	0.01	0.02	0.04	0.02	0.01	0.01	0.01	0.01	1.68	0.91	1.35	1.34	0.45	0.95

performed significantly better than the CNN model, which in turn performed significantly better than the MLP model (all $p < 0.035$).

The performance of both regression training strategies, evaluated in three different machine learning techniques, demonstrates that LMG data can be effectively used to predict finger motion. The statistical results indicate that the RF model is the most suitable architecture for this task, showing superior performance compared to CNN and MLP. In addition to its accuracy, RF is computationally efficient, requiring significantly fewer resources for training and deployment. This makes it well suited for embedded applications, such as prosthetic hands or rehabilitation devices, which typically rely on resource-constrained microprocessors for real-time control. Therefore, the combination of high accuracy and low computational cost makes RF a compelling choice for clinical and portable neuroprosthetic systems, enabling reliable and practical finger-motion decoding in real-world scenarios.

C. Limitations and Future Work

This study has several limitations that should be addressed in future research. First, the sample size was relatively small, consisting of only six able-bodied participants, and all experimental data was collected on the same day. Future studies should recruit a larger and more diverse cohort, including individuals with upper-limb amputations, and implement cross-subject validation protocols to better assess the generalizability of our findings. Second, the study utilized a limited set of grasp types and objects. Future research should expand the repertoire of hand movements and objects to evaluate the versatility and robustness of LMG-based decoding across a broader spectrum of functional tasks. Third, the current study focused on the offline prediction of finger motions from LMG data. While high offline accuracy was achieved, the online stability of this performance was not investigated. Future work should therefore focus on the real-time implementation of these decoding algorithms. This would allow for an assessment of their practical utility in applications such as controlling prosthetic or robotic hands by mapping the estimated finger motions to actuator commands. Moreover, since LMG demonstrates promising accuracy in both grasp classification and continuous finger motion regression, future work should focus on combining these two strategies. Specifically, a classification model could be used to select appropriate grasp-specific regressors for real-time prosthetic or robotic hand control.

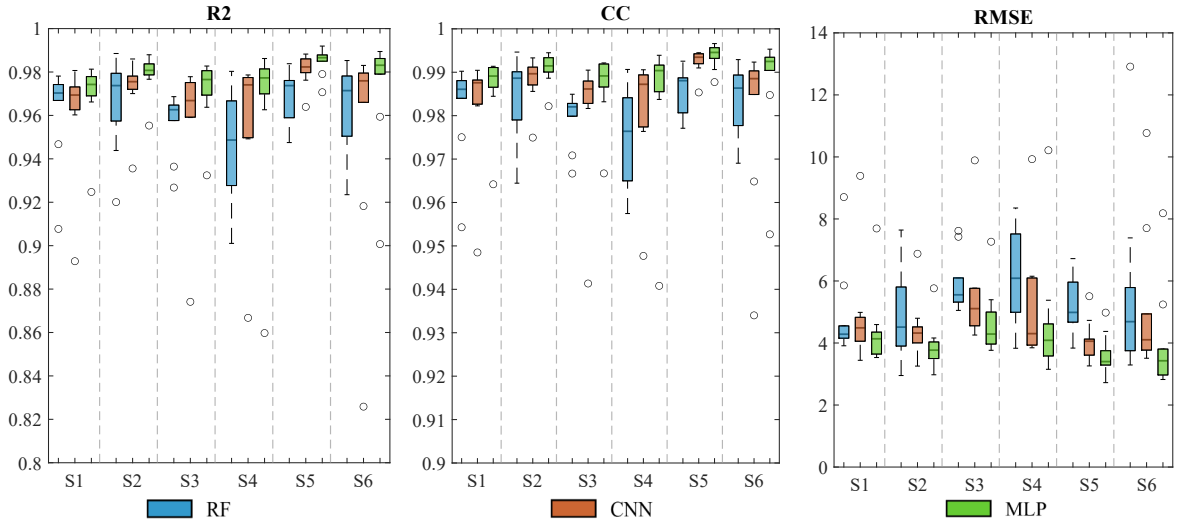

Fig. 9. Boxplots comparing the regression performance of the different decoding models for each subject, evaluated under three distinct metrics. Each boxplot shows the performance distribution generated from the scores of the ten cross-validation test folds.

TABLE IV

GENERALIZED REGRESSOR DECODING PERFORMANCE IN THREE METRICS. *AVG* STANDS FOR AVERAGE AND *STD* STANDS FOR SAMPLE STANDARD DEVIATION.

	R2						**CC**						**RMSE**					
	RF						**RF**						**RF**					
Subj.	**1**	**2**	**3**	**4**	**5**	**6**	**1**	**2**	**3**	**4**	**5**	**6**	**1**	**2**	**3**	**4**	**5**	**6**
AVG	0.96	0.97	0.96	0.94	0.97	0.95	0.98	0.98	0.98	0.97	0.99	0.97	4.82	4.80	5.89	6.18	5.22	5.57
STD	0.02	0.02	0.01	0.03	0.01	0.06	0.01	0.01	0.01	0.01	0.01	0.03	1.47	1.48	0.91	1.48	0.97	2.85
	CNN						**CNN**						**CNN**					
AVG	0.96	0.97	0.96	0.96	0.98	0.96	0.98	0.99	0.98	0.98	0.99	0.98	4.84	4.40	5.50	5.18	4.07	5.13
STD	0.03	0.01	0.03	0.03	0.01	0.05	0.01	0.01	0.01	0.01	0.01	0.02	1.67	0.99	1.63	1.89	0.65	2.33
	MLP						**MLP**						**MLP**					
AVG	0.97	0.98	0.97	0.96	0.98	0.97	0.99	0.99	0.99	0.98	0.99	0.99	4.39	3.87	4.67	4.69	3.40	3.96
STD	0.02	0.01	0.01	0.04	0.01	0.03	0.01	0.01	0.01	0.02	0.01	0.01	1.21	0.76	1.04	2.05	0.65	1.64

IV. CONCLUSION

This study investigated the effectiveness of lightmyography based Muscle-Machine Interfaces for the decoding of multi-finger motions and grasp types. To do so, both lightmyography and finger motion data were collected from six participants performing grasping tasks with five objects. Three machine learning algorithms were evaluated, and statistical analysis revealed distinct optimal models for each decoding task. For the prediction of multi-finger motions, the Random Forest model significantly outperformed both the Convolutional Neural Network and the Multi-Layer Perceptron, establishing it as the most suitable technique. The high accuracy achieved in motion prediction for both modeling strategies ($R^2 > 0.89, RMSE < 6.5°$) confirms that lightmyography is a powerful and viable modality for decoding complex motions. For the classification of hand grasp types, the Multi-Layer Perceptron proved to be the most effective model. While this work focused on offline analysis, the promising results establish a strong foundation for future research, particularly in the real-time implementation for applications such as prosthetic and robotic hand control. In summary, this research validates lightmyography as a robust, affordable, and effective alternative to traditional Muscle-Machine Interfaces for complex motion decoding tasks.

REFERENCES

[1] J. M. Hahne, M. A. Schweisfurth, M. Koppe, and D. Farina, "Simultaneous control of multiple functions of bionic hand prostheses: Performance and robustness in end users," *Science Robotics*, vol. 3, no. 19, p. eaat3630, 2018.

[2] E. Cho, R. Chen, L.-K. Merhi, Z. Xiao, B. Pousett, and C. Menon, "Force myography to control robotic upper extremity prostheses: a feasibility study," *Frontiers in bioengineering and biotechnology*, vol. 4, p. 18, 2016.

[3] X. Jiang, L.-K. Merhi, Z. G. Xiao, and C. Menon, "Exploration of force myography and surface electromyography in hand gesture classification," *Medical engineering & physics*, vol. 41, pp. 63–73, 2017.

[4] E. Krueger, E. M. Scheeren, G. N. Nogueira-Neto, V. L. d. S. N. Button, and P. Nohama, "Advances and perspectives of mechanomyography," *Revista Brasileira de Engenharia Biomédica*, vol. 30, pp. 384–401, 2014.

[5] Y.-P. Zheng, M. Chan, J. Shi, X. Chen, and Q.-H. Huang, "Sonomyography: Monitoring morphological changes of forearm muscles in actions with the feasibility for the control of powered prosthesis," *Medical engineering & physics*, vol. 28, no. 5, pp. 405–415, 2006.

[6] M. Shahmohammadi, A. Dwivedi, P. Nielsen, A. Taberner, and M. Liarokapis, "On lightmyography: A new muscle machine interfacing method for decoding human intention and motion," in *2021 43rd Annual International Conference of the IEEE Engineering in Medicine & Biology Society (EMBC)*. IEEE, 2021, pp. 4744–4748.

[7] B. Guan, R. V. Godoy, M. Shahmohammadi, A. Dwivedi, and M. Liarokapis, "Offline vs real-time grasp prediction employing a wearable high-density lightmyography armband: On the control of prosthetic hands," *IEEE Access*, 2025.

[8] M. Shahmohammadi, B. Guan, R. V. Godoy, A. Dwivedi, P. Nielsen, and M. Liarokapis, "On lightmyography based muscle-machine interfaces for the efficient decoding of human gestures and forces," *Scientific Reports*, vol. 13, no. 1, p. 327, 2023.

[9] B. Guan, R. V. Godoy, A. Dwivedi, and M. Liarokapis, "On the impact of different light wavelengths in decoding human intention in lightmyography controlled prosthetic hands," in *2025 47th Annual International Conference of the IEEE Engineering in Medicine and Biology Society (EMBC)*. IEEE, 2025, pp. 1–7.

[10] K. A. Abbas and M. T. Rashid, "Descriptive statistical features-based improvement of hand gesture identification," *Biomedical Signal Processing and Control*, vol. 92, p. 106103, 2024.

[11] J. P. Vásconez, L. I. B. López, Á. L. V. Caraguay, and M. E. Benalcázar, "A comparison of emg-based hand gesture recognition systems based on supervised and reinforcement learning," *Engineering Applications of Artificial Intelligence*, vol. 123, p. 106327, 2023.

[12] Z. Lu, S. Cai, B. Chen, Z. Liu, L. Guo, and L. Yao, "Wearable real-time gesture recognition scheme based on a-mode ultrasound," *IEEE Transactions on Neural Systems and Rehabilitation Engineering*, vol. 30, pp. 2623–2629, 2022.

[13] R. V. Godoy, B. Guan, A. Dwivedi, M. Shahmohammadi, M. Owen, and M. Liarokapis, "Multi-grasp classification for the control of robot hands employing transformers and lightmyography signals," in *2023 45th Annual International Conference of the IEEE Engineering in Medicine & Biology Society (EMBC)*. IEEE, 2023, pp. 1–6.

[14] H. Zhang, B. Peng, L. Tian, O. W. Samuel, and G. Li, "Continuous kalman estimation method for finger kinematics tracking from surface electromyography," *Cyborg and Bionic Systems*, vol. 5, p. 0094, 2024.

[15] K. Bimbraw, C. J. Nycz, M. Schueler, Z. Zhang, and H. K. Zhang, "Simultaneous estimation of hand configurations and finger joint angles using forearm ultrasound," *IEEE Transactions on Medical Robotics and Bionics*, vol. 5, no. 1, pp. 120–132, 2023.

[16] Z. Chen, H. Wang, H. Chen, and T. Wei, "Continuous motion finger joint angle estimation utilizing hybrid semg-fmg modality driven transformer-based deep learning model," *Biomedical Signal Processing and Control*, vol. 85, p. 105030, 2023.

[17] T. Feix, J. Romero, H.-B. Schmiedmayer, A. M. Dollar, and D. Kragic, "The grasp taxonomy of human grasp types," *IEEE Transactions on human-machine systems*, vol. 46, no. 1, pp. 66–77, 2015.

[18] F. Bach, "Batch normalization: Accelerating deep network training by reducing internal covariate shift," in *Proc 32nd Int Conf Mach Learn*, vol. 37, 2015, p. 448.

[19] M. A. Oskoei and H. Hu, "Myoelectric control systems—a survey," *Biomedical signal processing and control*, vol. 2, no. 4, pp. 275–294, 2007.

[20] K. Englehart and B. Hudgins, "A robust, real-time control scheme for multifunction myoelectric control," *IEEE transactions on biomedical engineering*, vol. 50, no. 7, pp. 848–854, 2003.

[21] T. K. Ho, "Random decision forests," in *Proceedings of 3rd international conference on document analysis and recognition*, vol. 1. IEEE, 1995, pp. 278–282.

[22] Y. LeCun and Y. Bengio, "Convolutional networks for images, speech, and time series," *The handbook of brain theory and neural networks*, 1998.

[23] D. P. Kingma, "Adam: A method for stochastic optimization," *arXiv preprint arXiv:1412.6980*, 2014.

[24] T. D. Wickens and G. Keppel, *Design and analysis: A researcher's handbook*. Pearson Prentice-Hall Upper Saddle River, NJ, 2004, vol. 860.

[25] J. Hsu, *Multiple comparisons: theory and methods*. CRC Press, 1996.